ISSN 1063-7826, Semiconductors, 2010, Vol. 44, No. 2, pp. 171–183. © Pleiades Publishing, Ltd., 2010.
Original Russian Text © A.P. Bakhtinov, V.N. Vodopyanov, Z.D. Kovalyuk, V.V. Netyaga, O.S. Lytvyn, 2010, published in Fizika i Tekhnika Poluprovodnikov, 2010, Vol. 44, No. 2, pp. 180–193.

SEMICONDUCTOR STRUCTURES, INTERFACES, AND SURFACES

Electrical Properties of Hybrid (Ferromagnetic Metal)–(Layered Semiconductor) Ni/*p*-GaSe Structures

A. P. Bakhtinov[a^], V. N. Vodopyanov[a], Z. D. Kovalyuk[a], V. V. Netyaga[a], and O. S. Lytvyn[b]

[a] *Frantsevich Institute of Materials Science Problems, Chernivtsi Branch, National Academy Sciences of Ukraine, ul. Vil'de 5, Chernivtsi, 58001 Ukraine*

^e-mail: chimsp@ukrpost.ua

[b] *Lashkarev Institute of Semiconductor Physics, National Academy Sciences of Ukraine, pr. Nauki 41, Kyiv, 03028 Ukraine*

Submitted June 30, 2009; accepted for publication July 10, 2009

Abstract—Two-barrier Ni/*n*-Ga_2Se_3/*p*-GaSe structures with nanoscale Ni-alloy grains caused by reactions at the "metal–layered semiconductor" interface were formed after growing Ni layers on the *p*-GaSe (0001) surface. Current–voltage and capacitance–voltage characteristics of hybrid structures were studied in the temperature range of 220–350 K. The dependence of the impedance spectra on the bias voltage was studied at various temperatures. The frequency dependences of the impedance at high frequencies ($f > 10^6$ Hz) are discussed in terms of the phenomena of spin injection and extraction in structures with an ultrathin spin-selective Ni/*n*-Ga_2Se_3 barrier and the effects of spin diffusion and relaxation in the semiconductor substrate. The room-temperature phenomena of the Coulomb blockade and negative differential capacitance were detected. These phenomena are explained based on an analysis of transport processes in a narrow region near the "ferromagnetic metal–semiconductor" interface, where nanoscale grains are arranged.

DOI: 10.1134/S1063782610020077

1. INTRODUCTION

The study of hybrid "ferromagnetic metal (FM)–nonmagnetic semiconductor (SC)" structures is an important area in semiconductor spintronics [1, 2]. The application potential of hybrid structures in spin devices is associated with the feasibility of efficient injection of spin-polarized electrons from FMs to high-resistivity SCs and their extraction from SCs to FMs in tunneling Schottky diodes at room temperature [3], as well as the use of the phenomena of tunneling magnetoresistance and Coulomb blockade in these structures [4]. Spin-polarized carrier accumulation, injection, diffusion, and drift in SCs can be studied by optical [5–7], electrical, [8], and impedance spectroscopy [9] methods.

In terms of technology, to increase the spin injection efficiency in hybrid structures, it is most important to fabricate a planar FM–SC contact with minimum roughness at the interface [1]. Atomically smooth Van der Waals (VdW) cleavage surfaces of layered semiconductor crystals (SCCs) feature a low density of surface states ($\lesssim 10^{10}$ cm^{-2}). They were used as model surfaces to study the interaction between atoms of contacting materials at the interface during the formation of barrier structures grown by "VdW epitaxy" [10] and vacuum deposition of metals [11]. Electrical properties of SCC-based heterostructures fabricated by deposition on an "optical contact" [12] and "nonmagnetic metal–layered SC" Schottky barriers (SBs) [13–18] were studied.

Thin GaSe epitaxial layers can be grown on Si (111) [19] and GaAs (001) [20] surfaces, which offers the possibility of developing new spintronic devices using conventional semiconductor technologies. The structure, morphology, and magnetic properties of the hybrid planar and granular nanoscale structures Fe(111)/GaSe(0001)/Si(111) [21] and Fe(111)/GaSe(0001)/GaAs(001) [22] were studied.

The electrical and magnetic properties of GaSe crystal doped with manganese [23] and intercalated with nickel [24] and cobalt [25] were studied. Electrical properties of hybrid "FM–layered SC" structures have barely been studied to date. In this paper, we present the results of a study of the structure, surface morphology, current–voltage (*I–V*) and capacitance–voltage (*C–V*) characteristics, and impedance of hybrid "FM–layered SC" (Ni/*p*-GaSe) structures.

2. SAMPLES AND EXPERIMENTAL TECHNIQUE

As substrates for growing hybrid structures, we used undoped GaSe crystals (ε polytype) grown by the Bridgman method. At $T = 300$ K, the resistivity of these crystals is $\sim 10^3$–10^4 Ω cm and the hole concentration is $p \approx 10^{14}$ cm^{-3}. To eliminate the effect of plastic deformation of SCC wafers on the results of the study, the substrate thickness was chosen ~300–500 μm. It is known that hydroxyl group adsorption on the VdW GaSe surface results in the formation of a

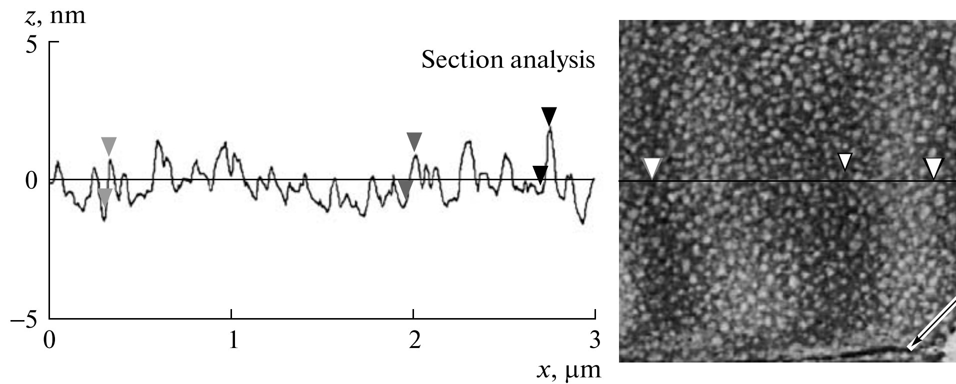

Fig. 1. Two-dimensional (2D) AFM image of the GaSe (0001) surface after depositing ten Ni monolayers and the height distribution of nanostructures along the horizontal line in the 2D image.

natural oxide consisting mostly of the Ga_2O_3 phase with SeO_2, $Ga_2(SeO_4)_3$, $Ga_2(SeO_3)_3 \cdot 6H_2O$, SeO_3, and Se_2O_5 inclusions [26]. This oxide was removed from the VdW GaSe surface after thermal annealing of substrates in a vacuum chamber in a 10% H_2 and 90% Ar atmosphere at $T = 200°C$ before metal deposition. Such technology allows desorption of not only low-temperature oxide components, but also the high-temperature Ga_2O_3 phase according to the chemical reaction

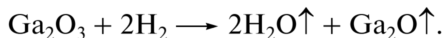

$$Ga_2O_3 + 2H_2 \longrightarrow 2H_2O\uparrow + Ga_2O\uparrow.$$

After annealing, the VdW surface structure was unchanged and gallium metal inclusions on this surface were not observed.

Nickel layers were deposited on the cleaned GaSe surface by electron-beam evaporation in vacuum. The layer deposition rate was 2×10^{-2} ML/s. One monolayer (ML) was 8×10^4 atom/cm^2 which corresponds to the surface density of GaSe atoms in the (0001) plane. The hybrid structure was formed by deposition through a circular hole (~1 mm in diameter) in a mask. After depositing the nickel layer (~90 nm thick), a thin gold layer was deposited (the work functions of these metals are almost identical, ~5.2 eV). A thin indium layer deposited on the opposite side of the GaSe(0001) substrate was used as an ohmic contact in the hybrid structure. Electrical taps from contacts in the FM–SC structure were formed using conductive silver paste.

I–V and *C–V* characteristics and impedance spectra of hybrid structures were studied using a Solartron FRA 1255 frequency analyzer in the frequency range of 10^{-1}–4×10^6 Hz at temperatures of 220–350 K. The voltage variation rate in measuring quasi-stationary *I–V* characteristics was ~5 mV/s. The dark transverse ac impedance was studied at a varied ac signal amplitude of ~10 mV and various dc bias voltages applied to contacts (In, Au) arranged along the *c* axis of the GaSe (0001) crystal. The nanostructure surface morphology was studied after depositing nickel layers of different thicknesses using a Nanoscope IIIa Dimension 3000SPM (Digital Instruments) atomic force microscope (AFM) in the tapping mode. X-ray diffraction analysis was performed using a DRON-3 X-ray diffractometer with CuK_α radiation ($\lambda = 1.5418$ Å) in the range $10° < 2\Theta < 60°$.

3. EXPERIMENTAL RESULTS AND DISCUSSION

3.1. Structure and Surface Morphology of Hybrid Ni/p-GaSe Nanostructures

The root-mean-square roughness determined by atomic-force microscopy (AFM) for the VdW GaSe (0001) surface before metal deposition is ~0.053 nm. In the AFM image of the Ni/*p*-GaSe nanostructure obtained after deposition of 10 ML of nickel (Fig. 1), a corrugated GaSe (0001) surface structure is observed, as well as three-dimensional nanoscale structures (NSs). The distances between linear wrinkles on the surface are l = 1–1.5 μm and their height is h = 1–1.5 nm. The lateral and vertical sizes of NSs are within x = 30–40 and z = 2–2.4 nm, respectively. During vacuum deposition of Ni, chemical reactions occur on the GaSe surface [27], which results in the formation of NSs in the upper SCC layers. Thermal expansion coefficients of the matrix and NSs are different. As a result of stress relaxations upon cooling of such structures from the growth temperature to room temperature, a corrugated SCC surface structure is formed [28]. This deformation process involves several SCC layers. Plastic flow of SCC deformation over pyramidal crystallographic planes of SCCs [29] is caused by cracking on the VdW surface (indicated by the long arrow in Fig. 1).

Chemical bonds between Ga and Se on the VdW GaSe (0001) surface are ruptured already after vacuum deposition of several iron [21] and nickel [27] MLs. The anisotropic SCC substrate poorly conducts heat in the direction perpendicular to the plane of (0001) layers. Upper GaSe layers are heated stronger

than the substrate bulk. At substrate temperatures above 300°C, gallium drops emerge on the GaSe surface [29]. The substrate temperature after Ni layer deposition ($d \approx 100$ nm) increased to $T_s = 270–350$°C when growing hybrid structures. It is known that stable compounds in the Ni–Ga system (Ga_4Ni_3, Ga_3Ni_2, Ni_3Ga, NiGa) are formed at temperatures above $T =$ 500–600°C [30]. At temperatures below 500°C, nickel forms stable compounds with chalcogens ($Ni_{1-x}Se_x$, $NiSe_2$) [31]. The insufficient sensitivity of the equipment used did not allow us to determine the chemical composition of NSs and their crystal structure.

The X-ray study of the hybrid Ni/*p*-GaSe structure after depositing the continuous Ni layer (~90 nm thick) showed that X-ray diffraction patterns, in addition to the diffraction peaks corresponding to the substrate ε-GaSe [26], include low-intensity Ni (200) reflection peaks and peaks corresponding to the GaSe δ polytype and α-Ga_2Se_3 compound (a defect crystal structure like zinc blende). The lattice parameters of the ε-GaSe substrate ($a = 3.754$ Å, $c = 15.982$ Å) were almost unchanged after depositing the Ni layer. This suggests that FM does not enter into VdW gaps in significant amounts during the formation of the hybrid Ni/*p*-GaSe structure. It is known that polytypes are formed in the GaSe SCC bulk after their thermal annealing in vacuum at temperatures lower than 600°C [32]. Two thermodynamically stable compounds, i.e., GaSe and Ga_2Se_3, exist in the Ga–Se system. Upon thermal annealing of SCCs, the formation of Ga_2Se_3 is preceded by intense defect formation and polytype phase transformations in these crystals. Thin intermediate *n*-Ga_2Se_3 layers almost always exist at heterointerfaces of *p*-GaSe-based structures obtained by thermal oxidation and control their electrical and photoelectrical properties [33]. The defect Ga_2Se_3 phase is characterized by high density of stoichiometric vacancies in the cation sublattice (~10^{21} cm^{-3}). This factor controls its anomalous properties with respect to the mechanism of the dopant entry into the lattice [34]. Introduction of magnetic ions into such defect structures can cause the formation of complex semiconductor compounds [21]. During growth of hybrid Ni/*p*-GaSe structures, NSs with complex composition (e.g., Ni–Ga_2Se_4) can be formed. We note that the formation of new phases was detected due to X-ray studies of Ni-intercalated GaSe crystals [24]. The band gap E_g of Ga_2Se_3 can vary from 1.8 to 2.6 eV, depending on the distribution of cation vacancies in crystallographic planes Ga_2Se_3 (001) [35, 36]. The nanoscale buffer Ga_2Se_3 layer is stable up to $T =$ 500–600°C. When growing hybrid structures Co:TiO_2/Si(001), it was used to prevent thermally activated diffusion from FM to SC [37].

The formation of hybrid Ni/*p*-GaSe nanostructures can be represented as follows. After depositing several Ni monolayers and chemical bond breaking

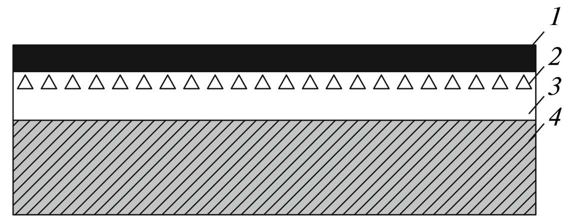

Fig. 2. Schematic representation of the Ni/*p*-GaSe hybrid structure: (*1*) Ni layer, (*2*) nanoscale structures, (*3*) *n*-Ga_2Se_3 layer, and (*4*) *p*-GaSe substrate.

between Ga and Se atoms, nanoscale drops of liquid gallium are formed on the VdW surface. The high diffusion rate of Ni adatoms on the VdW surface promotes their rapid arrival at Ga drops. The formation of NSs occurs in the presence of selenium in these drops [21]. Intense defect formation that occurs in upper SCC layers upon heating and a change in the gallium and selenium ratio promote the formation of a thin Ga_2Se_3 intermediate layer between FM and SCC. This defect phase prevents thermally activated diffusion of nickel to the SCC substrate during structure growth. The grown hybrid Ni/*p*-GaSe structure has the form schematically shown in Fig. 2.

3.2. Electrical Properties of the Hybrid Ni/p-GaSe Structure

Figure 3 shows the dark *I–V* characteristics of the hybrid Ni/*p*-GaSe structure measured at various temperatures. It is worth noting that the forward portions of these *I–V* characteristics correspond to the case where an external current source pole is connected to FM. This is characteristic of contacts between metals with large electron work functions and *n*-type SCs (e.g., Au/*n*-InSe [15]). When metals are in contact (Al, Au) with *p*-GaSe, the forward portions of *I–V* characteristics correspond to a negative polarity of voltage applied to metal [16, 17]. The current flow mechanism in the hybrid structure at small forward biases ($V < 0.5$ V) cannot be explained in terms of the thermionic emission theory. The forward portions of the *I–V* characteristic are nonlinear in the coordinates $\log J = f(V)$ (Fig. 3a). In the coordinates $\log J = f(\log V)$ (Fig. 2b), their shape is characteristic of the space-charge limited current (SCLC) mode. This mechanism takes place, e.g., in AuCr/*p*-Si SBs with β-$SiFe_2$ nanocrystals arranged in the diode space-charge region (SCR) [38]. It is caused by deep levels in the *p*-Si band gap. The slopes for linear regions of the *I–V* characteristic of the hybrid Ni/*p*-GaSe structure (Fig. 3b) are $n_1 = 2.21$ (at $V < 0.5$ V) and $n_2 = 1.42$ (at $V > 2$ V). They differ from the corresponding values $n_1 = 1$ and $n_2 = 2$ for the SCLC model of SBs with nanocrystals [38]. Reverse currents in the *I–V* characteristics of hybrid structures (Fig. 3a) increase with the reverse bias and temperature. The reverse currents for

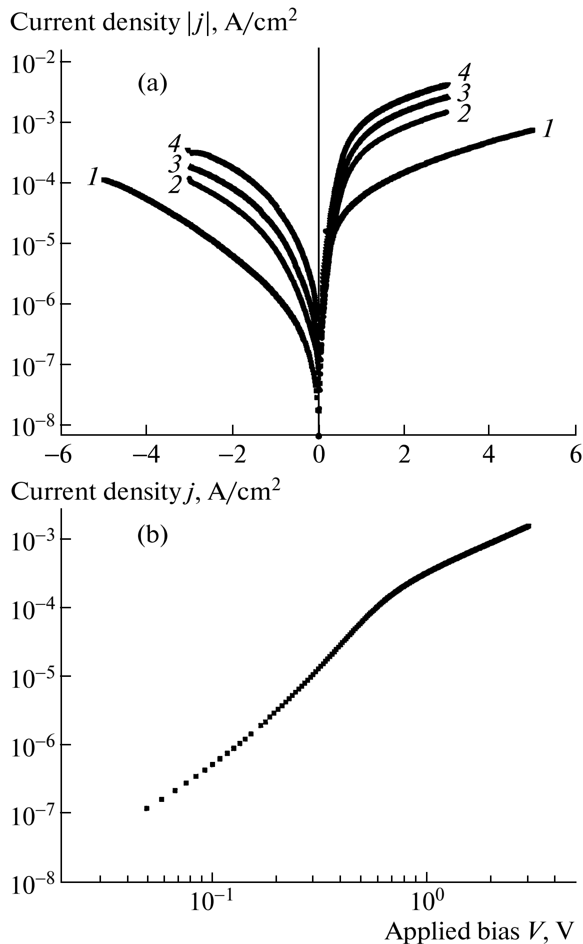

Fig. 3. (a) Current–voltage characteristics of the Ni/p-GaSe hybrid structure in the forward and reverse directions at temperatures $T = (1)$ 293, (2) 313, (3) 323, and (4) 343 K. (b) Current–voltage characteristic of the Ni/p-GaSe hybrid structure in the forward direction at $T = 293$ K. The forward direction corresponds to the external source plus connected to the Ni electrode.

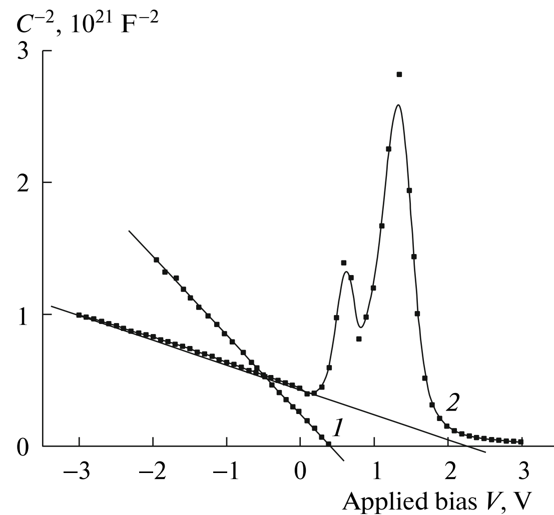

Fig. 4. Capacitance–voltage characteristics of the Ni/p-GaSe hybrid structure, measured at $T = 300$ K at frequencies $f =$ (1) 10^4 and (2) 10^6 Hz.

these structures exceed the calculated and experimental values for Au/p-GaSe:In [17] and Al/p-GaSe [16] SBs by more than an order of magnitude. Such a voltage dependence of the reverse current can be caused by the presence of lateral inhomogeneities at the FM–SC interface and carrier tunneling through the SB [39].

Figure 4 shows the C–V characteristics of Ni/p-GaSe structures measured at frequencies of 10^4 and 10^6 Hz at $T = 300$ K. Under reverse bias, these dependences are linear in the coordinates $C^{-2} = f(V)$. The C–V characteristics of hybrid structures depend on the frequency, which is observed for the structures based on layered SCs in the presence of an intermediate layer at the interface [40]. As the ac signal increases, the C–V characteristic slope decreases. Such behavior cannot be explained by deep impurity levels, since the contribution of defects with deep impurity levels to the SB capacitance in SCCs at $T = 300$ K appears at frequencies below 10^3 Hz [14, 41]. In the C–V characteristic of the hybrid structure measured at $T = 300$ K at a frequency of 10^6 Hz, extrema are observed at $V = 0.6$ and 1.4 V in the forward bias range $0.2\ \text{V} < V < 2\ \text{V}$ (Fig. 4, curve 2). States at the "nonmagnetic metal–layered SC" SB heterointerface do not contribute to the capacitance under forward bias in the frequency region $f > 2 \times 10^5$ Hz [18]. The extrema in the C–V characteristics of hybrid structures can be caused by the features of spin-polarized current flow in such structures [3] and NS recharging processes [42, 43].

The hybrid structure Ni/p-GaSe can be represented as a two-barrier structure consisting of the in series connected Ni/n-Ga_2Se_3 SB (with NSs embedded in the SCR) and the n-Ga_2Se_3/p-GaSe heterojunction (Fig. 5). The absence of accurate data on the band parameters and electron affinity for Ga_2Se_3 do not allow construction of an accurate energy-level diagram of the hybrid structure.

In this study, carrier transport phenomena in this structure are analyzed based on the energy-level diagram shown in Fig. 5. To this end, we used the impedance spectroscopy technique for semiconductor structures [44].

The total complex impedance of the barrier structure can be written as $Z^* = Z' - jZ''$, where Z' and Z'' are the real and imaginary parts of the impedance, respectively. The equivalent circuit of the barrier structure applied to analyze impedance spectra $Z'' = f(Z')$ is a parallel ($R_d \parallel C_d$) circuit connected in series with the resistance R_s. The latter accounts for the ohmic contribution of the substrate bulk, lead wires, and contacts; C_d is the structure barrier capacitance; and R_d is the equivalent parallel resistance of the structure. The

equivalent circuit for the hybrid structures under study consists of two in series connected ($R \| C$) circuits and resistance R_s (Fig. 6a). The Nyquist diagrams obtained at a zero bias of the hybrid structure at various temperatures are shown in Fig. 6b. We can see that they represent a superposition of two semicircles shifted with respect to each other along the Z' axis. This suggests that two relaxation processes occur, which are characterized by different relaxation times $\tau_d = R_d C_d$ at a given temperature, where $R_1C_1 > R_2C_2$. The larger semicircle is observed at $T = 300$ K in the frequency region $f < 3 \times 10^5$ Hz and is characterized by the values $R_1 = 2.3 \times 10^5\ \Omega$, $C_1 = 5.4 \times 10^{-11}$ F, and $\tau_1 = 1.24 \times 10^{-5}$ s. The smaller semicircle (see the inset in Fig. 6b) arranged in the region of higher frequencies is characterized at $T = 300$ K by the parameters $R_2 = 9.2 \times 10^3\ \Omega$, $C_2 = 4.9 \times 10^{-11}$ F, and $\tau_2 = 4.5 \times 10^{-7}$ s. As the temperature increases, semicircles shift along the Z' axis to higher frequencies and their diameters decrease. A decrease in R_1 and R_2 with increasing temperature is characteristic of semiconductor structures. In the low-frequency region ($f < 2 \times 10^3$ Hz), the real part of the impedance Z' is independent of frequency and decreases with temperature (Fig. 6c). The hybrid structure conductance in this frequency region is controlled by the substrate conductivity. The temperature dependence of this conductance exhibits activation behavior. The activation energy $E_a = 0.31$ eV determined from the temperature dependence of the resistivity $\rho \propto \exp(E_a/k_B T)$ is in good agreement with the data for undoped GaSe [13]. The relaxation process in the barrier structure, which is characterized by the relaxation time τ_1, corresponds to the maximum in the frequency dependence of Z'' (Fig. 6d).

The study of the impedance evolution at various biases and temperatures makes it possible to identify components of the complex barrier structure and to determine current flow mechanisms in each component [45]. Figures 7–10 show the Nyquist and Bode diagrams for the studied hybrid structure at various temperatures and bias voltages. The positive bias ($V > 0$) corresponds to the case where the FM electrode of the structure is positively biased with respect to the ohmic contact to the GaSe substrate, and the negative bias ($V < 0$) corresponds to the opposite case.

At $V > 0$, the Ni/n-Ga_2Se_3 SB and n-Ga_2Se_3/p-GaSe heterojunction are forward and reverse biased, respectively. At $V = 100$ mV and $T = 300$ K, the impedance spectrum $Z'' = f(Z')$ represents a superposition of various relaxation processes occurring in structure elements (Fig. 7a, spectrum *1*). An increase in the positive bias voltage results in a pronounced transformation of the impedance spectrum. The Nyquist diagrams at $V = 200$ mV and $T = 293$ K contain three regions (A, B, C) corresponding to different relaxation processes (Fig. 7a, spectra *2* and *3*). We can see in the frequency characteristic of the phase angle $\theta = f(\log f)$

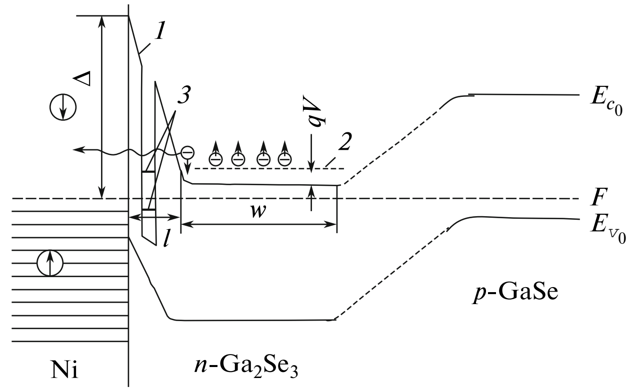

Fig. 5. Energy-level diagram of the Ni/n-Ga_2Se_3/p-GaSe hybrid structure: F is the Fermi level, Δ and l are the height and thickness of the spin-selective barrier at the Ni/n-Ga_2Se_3 heterointerface in the presence of a δ-doped semiconductor layer; (*1*) the Schottky barrier in the state of thermodynamic equilibrium, (*2*) extraction of spin-polarized ($\sigma = \downarrow$) electrons from semiconductor to Ni under forward bias ($V > 0$) of the hybrid Schottky barrier [48], and (*3*) spatial quantization levels of nanoscale structures.

(Fig. 8), where $\theta = \arctan(Z''/Z')$, that these processes correspond to the resonant frequencies $f_1 = 5 \times 10^4$ Hz (region A) and $f_2 = 10^6$ Hz (region B). The third relaxation process is observed in the high-frequency spectral region $f_3 > 10^6$ Hz (region C). The resonant frequency f_3 for this process is outside the frequency range under study. As the voltage increases $V > 0$, the semicircle diameter in the region B strongly decreases (spectrum *3* in Fig. 7a). This corresponds to a decrease in the ohmic resistance R_2 of the ($R_2 \| C_2$) circuit for the Ni/n-Ga_2Se_3 SB. As the positive bias voltage varies from $V = 0.1$ to $V = 0.6$ V, R_2 decreases from $\sim 10^4$ to $5 \times 10^2\ \Omega$. Such behavior of the dependence $Z'' = f(Z')$ under forward bias is characteristic of SBs with an intermediate layer at the metal–SC interface, which is tunnel-transparent for carriers [45]. The weak temperature dependence of the resonant frequency f_2 also argues in favor of the tunneling mechanism of current flow through the SB [44]. The ohmic resistance R_1 of the ($R_1 \| C_1$) circuit for the reverse biased heterojunction n-Ga_2Se_3/p-GaSe decreases with the bias voltage in the range $0.1 < V < 0.2$ from 5×10^4 to $2 \times 10^3\ \Omega$ and remains almost unchanged as the voltage further increases to $V = 3$ V (Fig. 7a). The position $f_1 = 1/2\pi R_1 C_1$ of the maximum in the Bode diagrams (Fig. 7c) depends on the temperature and shift. In the case of decreasing T and an almost unchanged bias voltage ($V = 0.2$–0.3 V), it shifts to lower frequencies, which is caused by an increase in R_1. At a constant temperature ($T = 300$ K) and an increasing bias, the maximum f_1 shifts to the high-frequency region from $f_1 = 5 \times 10^4$ Hz (at $V = 0.2$ V) to $f_1 = 2 \times 10^5$ Hz (at $V = 3$ V) (Fig. 8). This is due to broadening of the hetero-

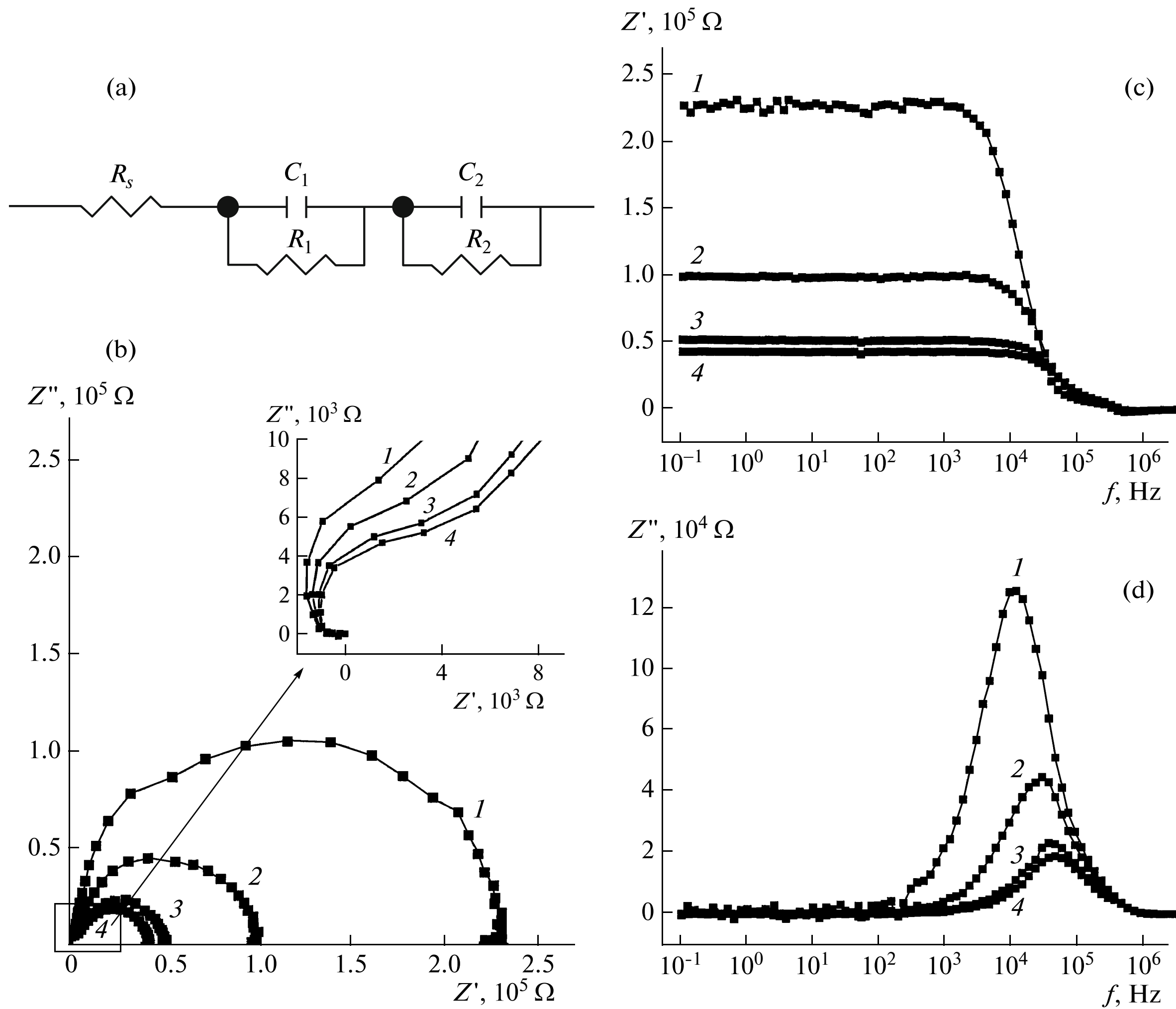

Fig. 6. (b–d) Impedance spectra of the Ni/*p*-GaSe hybrid structure, measured under zero bias ($V = 0$) at temperatures $T =$ (*1*) 293, (*2*) 313, (*3*) 323, and (*4*) 343 K. (a) Equivalent circuit of the Ni/*p*-GaSe hybrid structure; (b) Nyquist diagrams. The inset shows the magnified high-frequency region of diagrams. (c) Frequency dependences of the real part Z' of the total complex impedance; (d) frequency dependences of the imaginary part Z'' of the total complex impedance.

junction SCR and decreasing the capacitance C_1. The relaxation process in region *A* (Fig. 7a) is caused by the tunneling–recombination mechanism of current flow, which takes place in the SCC heterojunction [12].

The relaxation processes observed in the high-frequency region *C* ($f > 10^6$ Hz) of the impedance spectrum at $V > 0$ can be caused by accumulation and diffusion of spin-polarized electrons in the hybrid structure. In hybrid FM–(*n*-type SC) SBs, injection of spin-polarized electrons from FM into SC occurs under reverse biases; extraction of spin-polarized electrons from SC takes place under forward biases if the barrier to these carriers is low (lower than 200 mV) [46]. For efficient injection/extraction of spin-polarized electrons, a "spin-selective barrier" is formed at the FM–SC interface [3], which contains a thin δ-doped SC layer [7, 47, 48]. This layer should be very thin to provide tunneling of spin-polarized electrons through the barrier at low bias voltages (on the order of about several k_BT, where k_B is the Boltzmann constant). For nickel at $T = 300$ K, states of spin-polarized electrons with spin $\sigma = \uparrow$ are populated and are below the Fermi level *F*. States of spin-polarized electrons with spin $\sigma = \downarrow$ are above the Fermi level [2]. As the voltage $V > 0$ applied to the Ni/(*n*-type SC) hybrid structure increases, electrons with spins $\sigma = \downarrow$ are extracted from SC and electrons with spins $\sigma = \uparrow$ are accumulated in SC near the FM–SC interface. Calculations show that a high degree of spin polarization in SC can be achieved at $T = 300$ K under forward bias of the SB based on high-resistivity SC with a modified barrier [48]. Since the spin relaxation time for electrons in SC can reach $\sim 10^{-9}$ s at this temperature [2, 3], relaxation processes involving these carriers should manifest themselves in the high-frequency region of the impedance spectrum ($f > 10^6$ Hz) [9]. At $T = 300$ K, electron

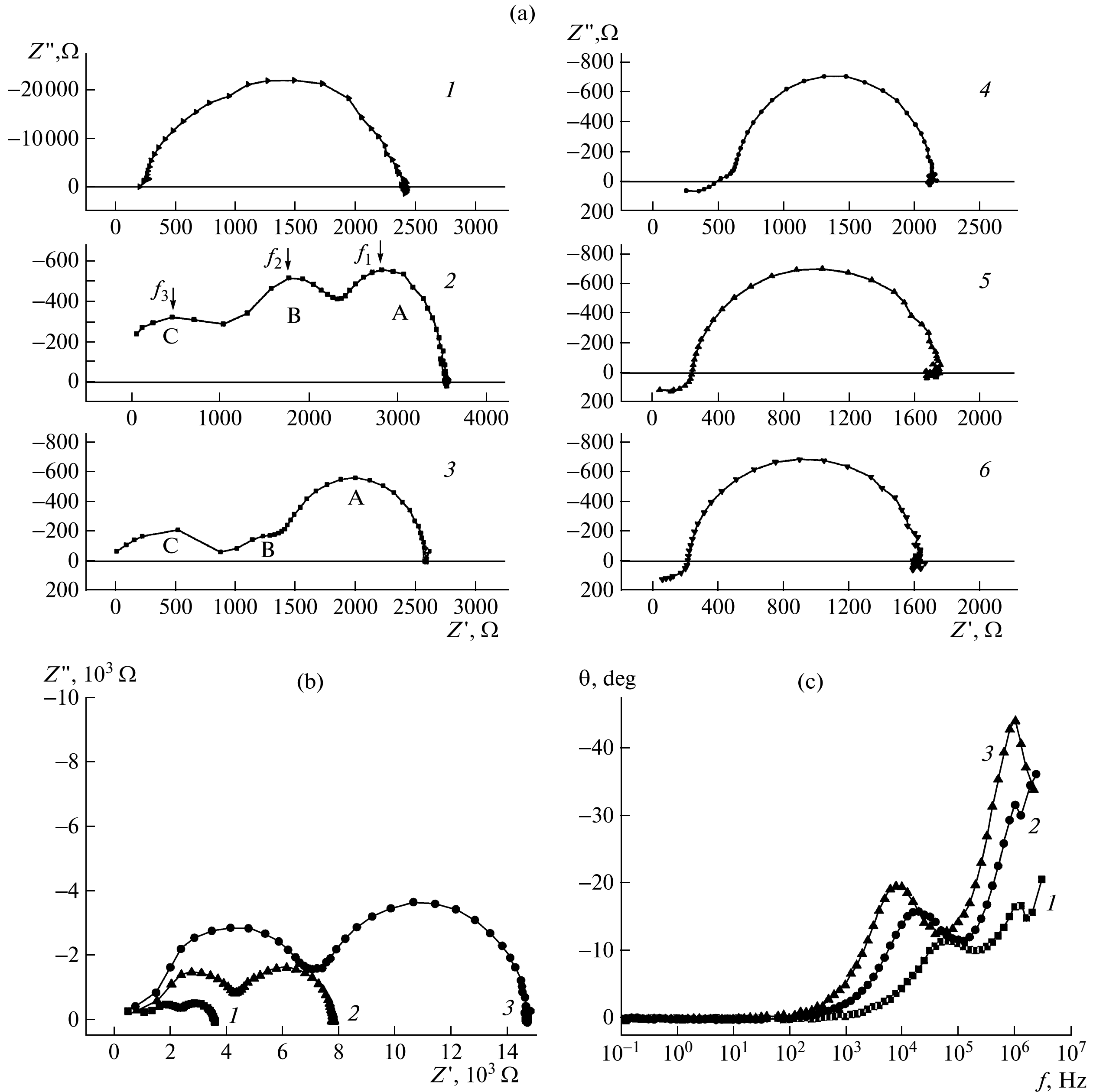

Fig. 7. Impedance spectra of the Ni/p-GaSe hybrid structure, measured at various positive bias voltages ($V > 0$). The bias voltage sign corresponds to the external current source plus connected to the Ni electrode. (a) Nyquist diagrams at the temperature T = 293 K and bias voltages of (*1*) 0.1, (*2*) 0.2, (*3*) 0.3, (*4*) 0.8, (*5*) 2.5, and (*6*) 3 V; (b) Nyquist diagrams $Z''=f(Z')$; (c) the frequency dependences of the phase angle θ at temperatures T = (*1*) 293, (*2*) 253, and (*3*) 240 K. Measurements were performed at bias voltages V = (*1*) 0.2, (*2* and *3*) 0.3 V.

tunneling through the spin-selective barrier from n-Ga_2Se_3 in Ni and the appearance of the high-frequency impedance component in region C is observed already at a positive bias voltage $V = 0.2$ V. This voltage is redistributed between the hybrid structure components R_1, R_2, and R_s. We can see in the Nyquist diagrams (Fig. 7b) that the resistances R_1 and R_2 are approximately equal and higher than R_s. This means that electron tunneling from SC into FM in the Ni/n-Ga_2Se_3 SB occurs at a forward bias voltage $V < 0.1$ V applied to the SB. The fulfillment of this requirement is necessary for efficient spin injection/extraction in FM–SC hybrid diode structures [46–48]. Upon cooling of the hybrid structure to T = 240 K (Fig. 7b), the relaxation processes associated with electron tunneling through a thin barrier occur at higher positive voltages (V = 0.3 mV) applied to the hybrid structure. This may be caused by an increase in the structure resistances R_1, R_2, and R_s (semicircle diameters in Fig. 7b). In the high-frequency region C of the impedance spectrum,

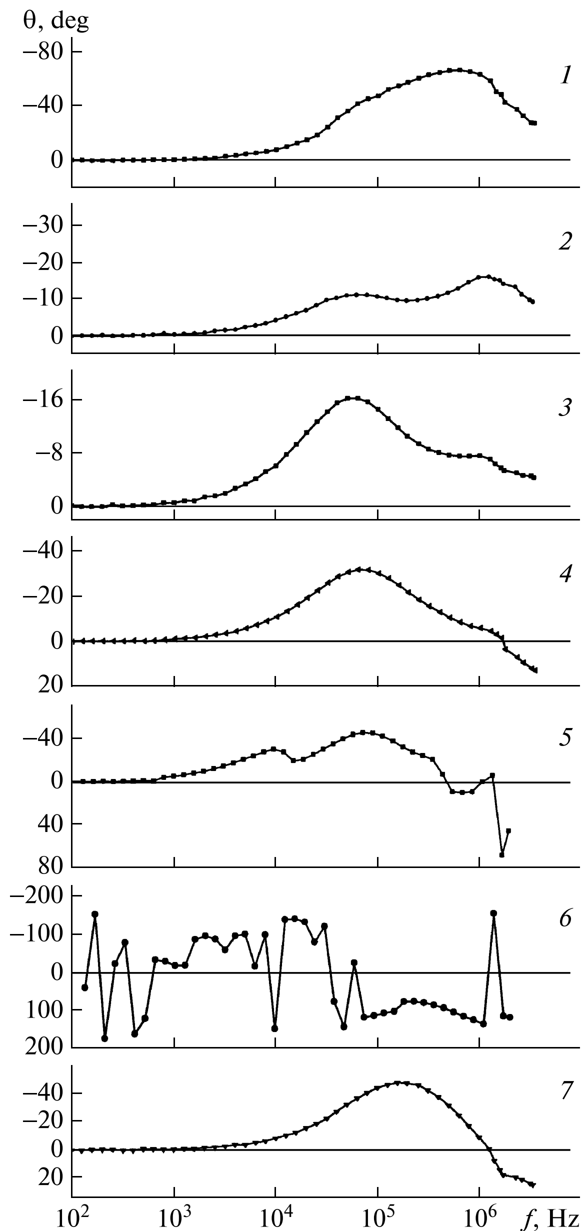

Fig. 8. Frequency dependences of the phase angle θ at temperature T = 293 K and bias voltages V = (*1*) 0.1, (*2*) 0.2, (*3*) 0.3, (*4*) 0.8, (*5*) 1.4, (*6*) 1.5, and (*7*) 3.0 V.

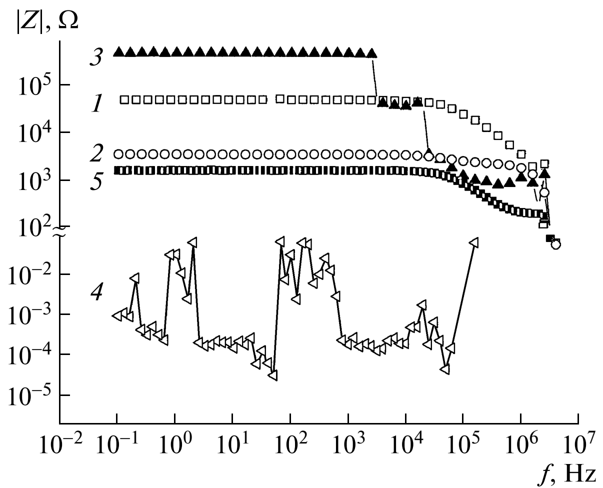

Fig. 9. Frequency dependences of the total impedance magnitude $|Z|$ at temperature T = 293 K and bias voltages V = (*1*) 0.1, (*2*) 0.2, (*3*) 1.4, (*4*) 1.5, and (*5*) 3.0 V.

the imaginary impedance part $Z'' \propto 1/\omega C$ is positive and decreases as bias increases from 0.2 to 0.6 V. In this case, the phase angle decreases in this frequency range (Fig. 8). Such changes in the capacitance component of the impedance and the phase angle may be associated with accumulation of spin-polarized electrons with spin $\sigma = \uparrow$ in n-Ga_2Se_3 near the FM–SC heterointerface. These electrons are localized in the SC region characterized by the size $L \le l_S$, where l_S is the electron spin diffusion length in SC [2, 3]. Diffusion and drift of spin-polarized electrons in the FM–SC hybrid structure under forward bias depend on the bias voltage and SC layer thickness [49]. As the bias voltages increases $V > 0$, the concentration of accumulated spin-polarized electrons $\sigma = \uparrow$ in n-Ga_2Se_3 increases, and the SCR width of the n-Ga_2Se_3/p-GaSe heterojunction increases. The spin diffusion current is directed from the FM–SC interface to the SC bulk [50]. If the n-Ga_2Se_3 layer thickness $w < L$, accumulated spin-polarized electrons can tunnel through states at the n-Ga_2Se_3/p-GaSe heterojunction to the hole-depleted p-GaSe substrate region. Diffusion of these minority carriers to p-GaSe can cause Z'' and θ sign changes that occur at $V > 0.6$ V (Figs. 7a and 8). In the general case, the negative imaginary impedance $Z'' < 0$ is caused by the phase shift between the ac-signal voltage and current in the presence of the “negative” capacitance in the electric circuit [51]. The correct interpretation of the “negative” capacitance effect is based on the analysis of frequency dependences of the impedance [44]. The effects associated with the “negative” capacitance in quantum-well infrared detectors (QWIPs) are caused by transient processes during level recharge in quantum wells [51]. In MOS tunnel diodes (MOSTDs), the “negative” capacitance effect occurs during minority carriers’ injection into SC and is associated with SC conductivity modulation [45]. The diffusion “negative” capacitance in SBs, which is associated with minority carriers’ diffusion in SC, depends on the forward bias voltage and is connected in parallel with the SCR capacitance [52]. These effects occur in the low-frequency region of the impedance spectrum ($f < 10^6$ Hz). The negative imaginary impedance in heterojunctions containing nonmagnetic nanocrystals in the SCR is caused by charge accumulation on heterointerfaces between nanocrystals and matrix. It is observed in the low-frequency range ($f = 10^3$–10^4 Hz) [53]. The capacitance of the

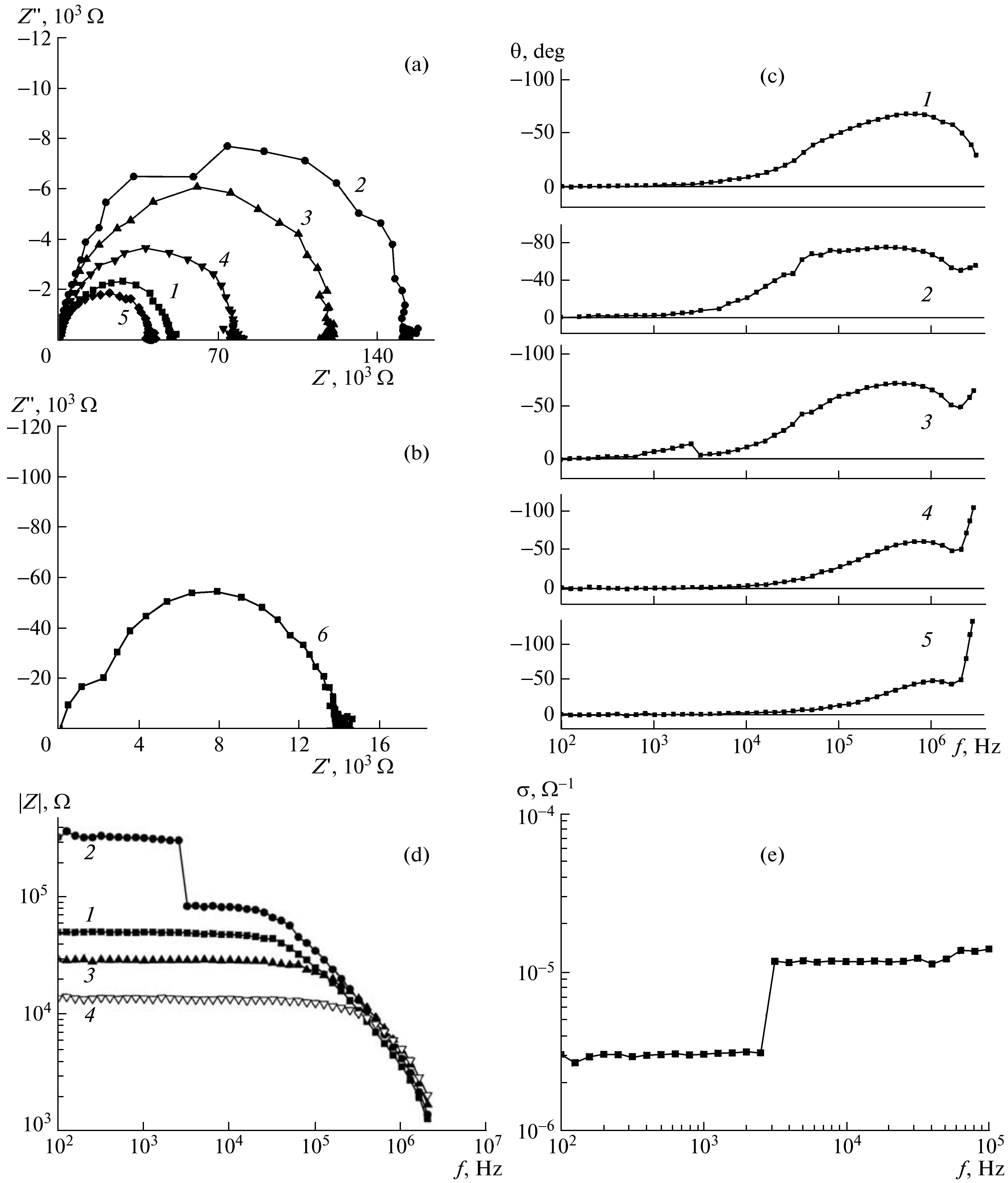

Fig. 10. Impedance spectra of the Ni/*p*-GaSe hybrid structure measured at $T = 293$ K and at various negative bias voltages ($V < 0$). The bias voltage sign corresponds to the external current source minus connected to the Ni electrode. (a, b) Nyquist diagrams at bias voltages $-V =$ (*1*) 0, (*2*) 0.25, (*3*) 0.5, (*4*) 0.8, (*5*) 1.5, and (*6*) 3.0 V; (c) frequency dependences of the phase angle θ at bias voltages $-V =$ (*1*) 0, (*2*) 0.25, (*3*) 0.7, (*4*) 1.8, and (*5*) 3.0 V; (d) frequency dependences of the total impedance magnitude $|Z|$ at bias voltages $-V =$ (*1*) 0, (*2*) 0.7, (*3*) 1.8, and (*4*) 3.0 V; (e) frequency dependence of the real part of the conductance at $V = -0.7$ V.

"nonmagnetic metal–layered SC" SB approaches a constant value ("geometrical capacitance" [44]) with increasing frequency for SBs based on other SCs in the high-frequency region [51]. In the frequency range $f = 10^5$–10^6 Hz, this capacitance decreases, which is caused by the large series resistance R_s of the SCC substrate, and remains constant at frequencies exceeding 10^6 Hz [18].

Nanoscale structures (NSs) in the n-Ga_2Se_3 matrix can be considered as a set of noninteracting quantum dots (QDs) that can trap carriers. The capacitance of the Schottky diode with a QD plane embedded into the SCR is

$$C = C_{3D} + C_{qd},$$

where C_{3D} and C_{qd} are the 3D and 2D components [42]. As the voltage increases $V > 0$, size quantization levels of NSs are sequentially filled with electrons. The significant difference between resistances R_1 and R_2 ($R_2/R_1 \ll 1$) provides a gradual shift of size quantization levels of QDs with respect to the Fermi level as the voltage applied to the hybrid structure changes by ~100 mV. As is known, if the rate of thermal emission of electrons from QDs is lower than the frequency ω of the measuring ac signal, the quantum component of the capacitance is suppressed in SBs with QDs [42]. The maximum at $V = 1.4$ V and $f = 10^6$ Hz in the C–V characteristic in the coordinates $C^{-2} = f(V)$ (or the corresponding minimum in the coordinates $C = f(V)$, where the negative differential capacitance is observed) is the manifestation of the zero-dimensional nature of QD states [42, 54]. This effect is associated with QD recharge processes [42, 43]. At $V = 1.4$ V, the frequency dependence of the impedance magnitude (Fig. 9) exhibits discrete steps in the frequency ranges $f = 2.5$–3.1, 20–25 kHz, and 1.0–2.0 MHz, which are characteristic of transport processes that occur involving discrete levels in SC QDs. In this case, significant changes in the phase angle θ are observed associated with QD level recharge (Fig. 8). We note that deep defect levels in SC structures usually appear in the frequency dependences of the impedance magnitude as broad maxima [55]. In the bias range 1.4 V $< V <$ 2 V, pronounced periodic changes in the impedance magnitude are observed,

$$|Z| = [(Z')^2 + (Z'')^2]^{1/2}, \quad (1)$$

which depend on the applied voltage (Fig. 9). We can see that the hybrid structure conductance in the low-frequency region of the impedance spectrum ($f <$ 1 kHz) changes by several orders of magnitude as the bias voltage V changes by ~0.1 V. Such conductance changes can be associated with the "Coulomb blockade" phenomenon [56]. This effect is observed in structures with SC QDs at low temperatures if QDs are small and their electrostatic energy $E_c = e^2/2C$ is higher than the thermal fluctuation energy k_BT, where e is the electron charge and C is the QD capacitance. The charge accumulated by a QD array depends on the voltage, temperature, density of states in QDs, and the electrostatic potential of the region in which they are arranged [42, 54]. For example, the periodic potential of the GaAs/AlAs superlattice in SBs with InAs QDs results in an increase in the energy required for electron exchange between the QD and GaAs conduction band [54]. In such structures, the effect of the negative differential capacitance under forward bias is observed at temperatures close to room temperature [43]. The Coulomb blockade at room temperature was also observed in MOS structures on silicon with oxidized Ge QDs [57].

At positive biases $V < 1.4$ V applied to the hybrid structure under study, electrons tunnel from n-Ga_2Se_3 to Ni through a spin-selective barrier on surface areas of the FM–SC interface, which are arranged between NSs. Low-dimensional structures in the n-Ga_2Se_3 matrix are in the electric field induced by accumulated spin-polarized electrons $\sigma = \uparrow$. In the case of extraction of spin-polarized electrons from SC under forward bias, the capacitance of the hybrid Schottky diode with QDs includes three in-parallel connected components: C_{3D}, C_{qd}, and the capacitance C_{acc} caused by accumulated electrons $\sigma = \uparrow$. As the temperature decreases, the peak of the negative differential capacitance in the C–V characteristic of the SB with QDs under forward bias shifts to higher voltages [43]. Upon cooling of the Ni/n-Ga_2Se_3/p-GaSe hybrid structure from $T = 300$ to 253 K, the features in the frequency dependences of the impedance magnitude and the effect of the negative differential capacitance in the C–V characteristic were also observed at higher bias voltages ($V \approx 2.0$ V). At $T = 300$ K and $V \geq 1.4$ V, a additional contribution to the current through the hybrid structure can be made by electrons tunneling through NSs and the Ni/n-Ga_2Se_3 spin-selective barrier. These are unpolarized electrons coming from the In contact and spin-polarized electrons accumulated in n-Ga_2Se_3. We note that the quasi-Fermi level for accumulated electrons depends on the spin and coordinates [1–3]. Spin-polarized current flow through the SC QD connected to FM contacts depends on the relative magnetic (parallel or antiparallel) system configuration [56]. In the Coulomb blockade mode, sequential electron tunneling through the QD (the first-order process) is suppressed [58]. In this case, tunneling is performed through virtual states (the second-order process). The process of spin-polarized electron tunneling through the multilevel QD in the Coulomb blockade mode is accompanied by a strong increase in low-frequency noise observed in a certain voltage range [58]. This "superpoisson" [58] shot noise is associated with inelastic tunneling processes in the QD, which are accompanied by electron spin flip. In this case, an additional contribution to the low-frequency noise in the hybrid structure can be caused by electron spin fluctuations at the input of the spin filter (spin-selective barrier), which cause random variations in the current and current phase and are observed at $V = 1.5$ V (Figs. 8 and 9). If the QD is completely filled, spin-polarized electron transport through it results from elastic tunneling processes (without electron spin flip). In this case, the low-frequency noise does not increase. It is Poisson or "subpoisson" [58]. In the region of positive biases $V > 2.0$ V, quantum-size levels of NSs are arranged below the n-Ga_2Se_3 Fermi

level, and the low-frequency noise does not appear in the impedance spectra. The Nyquist diagrams (Fig. 7a) at such biases are shaped as semicircles. The relaxation process corresponding to electron tunneling through the Ni/n-Ga_2Se_3 SB is almost indistinguishable in these diagrams due to the low tunneling resistance R_2. The negative impedance in the high-frequency region C at T = 300 K and V = 2.5 V is described by a semicircle with the parameters R_3 = 234 Ω, $C_3 = 2.71 \times 10^{-10}$ F, and $\tau_3 = 6.3 \times 10^{-8}$ s; at V = 3.0 V, these parameters are R_3 = 221 Ω, $C_3 = 2.86 \times 10^{-10}$ F, and $\tau_3 = 6.3 \times 10^{-8}$ s. In this case, the "negative" capacitance increases with the positive bias. The impedance sign in the high-frequency spectral region under biases $V > 2.0$ V is unchanged. The relaxation process in this frequency region may be associated with diffusion of accumulated electrons in the p-GaSe substrate. The value of τ_3 for this process is larger than the relaxation time of electrical processes (~4×10^{-9} s), determined from the impedance spectra of composite structures with FM clusters [59]. The high-frequency component of the capacitance of composite structures is controlled by the processes of charge accumulation at interphase boundaries. For these structures, in contrast to the hybrid structures under study, it decreases with the bias voltage.

When describing the carrier transport in spintronic devices, diffusion and drift of unpolarized and polarized carriers, carrier recombination, and spin relaxation processes are taken into account [2]. The physical nature of the relaxation process observed in the high-frequency region of the impedance spectrum can be determined based on the results of the comprehensive study of the electrical impedance in the frequency region $f > 10^6$ Hz using electrical and optical methods for studying spin accumulation [5–8].

At $V < 0$, the Ni/n-Ga_2Se_3 SB and n-Ga_2Se_3/p-GaSe heterojunction are forward and reverse biased, respectively. In this case, spin-polarized electrons tunnel from FM to n-Ga_2Se_3 through the spin-selective barrier. At such a bias voltage, holes are injected from p-GaSe to n-Ga_2Se_3, where they recombine with electrons. The main contribution to the tunneling current in hybrid SBs with Ni contact is made by electrons $\sigma = \downarrow$; in this case, the degree of polarization P does not exceed ~40% [2]. At negative biases, features in the high-frequency region of the impedance spectrum ($f > 10^6$ Hz) are observed in the Nyquist diagrams (Figs. 10a and 10b) and the frequency dependences of the phase angle (Fig. 10c), as well as relaxation processes associated with current flow through circuits ($R_1 \parallel C_1$) and ($R_2 \parallel C_2$). At a negative bias $V = -0.7$ V applied to the structure, the frequency dependence of the impedance magnitude in the frequency range f = 2.5–3.1 kHz exhibits a step (Fig. 10d). It can be caused by emptying the NS energy level filled with electrons when it passes through the Fermi level of the n-Ga_2Se_3 matrix. As a testing ac voltage with frequency f is applied to the SB, the NS level begins to oscillate with respect to the Fermi level. In this case, electrons are emitted to the n-Ga_2Se_3 conduction band with which the change in the real part of the structure conductance is associated (Fig. 10e). We note that features in this frequency region were also observed in Bode diagrams during NS recharge at $V = 1.4$ V (Figs. 8 and 9). In the Nyquist diagrams, the semicircles corresponding to the processes in circuits ($R_1 \parallel C_1$) and ($R_2 \parallel C_2$) are partially overlapped. As the bias voltages increases to $V = -0.25$ V, the semicircles shift along the real axis to the region of high resistances (Figs. 10a and 10b). This is caused by an increase in the ohmic resistance R_2 of the ($R_2 \parallel C_2$) circuit under reverse bias of the Ni/n-Ga_2Se_3 SB from ~9.2×10^3 (at $V = 0$) to 1.5×10^5 Ω (at $V = -0.25$ V). As the negative bias voltage further increases, the semicircles shift in the opposite direction. Such behavior of the hybrid structure is associated with the appearance of the δ-shaped barrier at the FM–SC heterointerface, which becomes transparent for electron tunneling from FM to SC at low bias voltages. The resistance R_2 decreases from ~1.5×10^5 to ~10.6×10^3 Ω as $|V|$ increases from 0.25 to 3 V. In this case, the SCR of the Ni/n-Ga_2Se_3 SB broadens and the capacitance C_2 decreases from ~4.9×10^{-11} to ~3.3×10^{-11} F. The ohmic resistance R_1 of the ($R_1 \parallel C_1$) circuit of the n-Ga_2Se_3/p-GaSe heterojunction at such a change in the bias voltage decreases from ~2.3×10^5 to ~1.2×10^3 Ω. At such a bias voltage polarity, a relaxation process is observed in the high-frequency region of the impedance spectrum ($f > 10^6$ Hz) (Figs. 10a and 10b). It is pronounced as the current through the structure increases (at $V = -3$ V). The phase angle θ for this process is positive at all bias voltages. The Ni/n-Ga_2Se_3/p-GaSe hybrid structure is an analogue of spin light-emitting diodes (spin-LED heterostructures) [3, 7] in which spin-polarized electrons are injected under reverse bias of hybrid SBs. The bias voltage has a significant effect on the efficiency of spin injection of electrons from FM to SC [47], the electron–hole recombination time τ_r, and the time of electron spin relaxation τ_S [2, 3]. The efficiency of spin injection at $V < 0$ in the hybrid structures under study can be determined by studying the polarization electroluminescence of these structures in a magnetic field [6].

4. CONCLUSIONS

The surface structure and morphology of layered GaSe crystals after vacuum deposition of ferromagnetic metal Ni layers are studied. It was found that the chemical and deformation interaction between deposited atoms and the substrate results in the formation of a thin layer of damaged Ga_2Se_3 SC in upper GaSe layers. This intermediate layer is arranged between FM and GaSe and contains NSs being a product of chem-

ical reactions. The electrical properties of the grown Ni/n-Ga_2Se_3/p-GaSe hybrid structure were studied at various temperatures and bias voltages. As a result of the study of the frequency dependences of the impedance, relaxation processes associated with current flow through the Ni/n-Ga_2Se_3 SB and n-Ga_2Se_3/p-GaSe heterojunction were detected. At $T = 300$ K, electron tunneling from n-Ga_2Se_3 to FM (at $V > 0$) and from FM to n-Ga_2Se_3 (at $V < 0$) is observed at low bias voltages (lower than 0.25 V) applied to the structure. This indicates the existence of a Ni/n-Ga_2Se_3 barrier tunnel-transparent for electrons, which could result from impurity segregation in a thin layer of defect Ga_2Se_3 SC. The process of electron tunneling from n-Ga_2Se_3 through this barrier at $V > 0$ is accompanied by charge accumulation in the SCR of Ni/n-Ga_2Se_3 and appears as a relaxation process in the high-frequency region of the impedance spectrum ($f > 10^6$ Hz). This process can be associated with accumulation of spin-polarized electrons $\sigma = \uparrow$ in n-Ga_2Se_3, which occurs during extraction of electrons $\sigma = \downarrow$ from n-Ga_2Se_3 to FM through a narrow δ-shaped barrier (spin filter). The negative impedance observed in the frequency region $f > 10^6$ Hz at $V > 2$ V and characterized by the relaxation time 6.3×10^{-8} s can be caused by diffusion of these accumulated electrons in the p-GaSe substrate. At $V < 0$, spin-polarized electrons tunnel from FM to the n-Ga_2Se_3 conduction band and recombine with unpolarized holes injected from p-GaSe. The positive impedance corresponding to this process is clearly observed in the Nyquist diagrams in the frequency region $f > 10^6$ Hz at negative bias voltages higher than 1.8 V. It was found that the presence of NSs in the SCR of Ni/n-Ga_2Se_3 has an effect on room-temperature current flow in the hybrid structure. The effect of the negative differential capacitance associated with NS recharge is observed in the C–V characteristic of the hybrid structure at $V > 0$ and at the measuring signal frequency $f = 10^6$ Hz. The NS recharge processes at this bias are also reflected in Bode diagrams. A change in the hybrid structure conductance was detected in the low-frequency spectral range $f = 2.5$–3.1 kHz under reverse bias of the Ni/n-Ga_2Se_3 SB. This effect is explained by emptying the NS spatial quantization level which was filled at $V = 0$ when it passes through the n-Ga_2Se_3 Fermi level. Strong periodic changes in the impedance magnitude were detected at $1.4 \text{ V} < V < 2$ V, which may be caused by the Coulomb blockade of electron tunneling from n-Ga_2Se_3 through NSs. Strong fluctuations in the phase angle and impedance magnitude of Ni/n-Ga_2Se_3 in the low-frequency spectral region at certain positive biases (low-frequency noise) can be caused by tunneling features of spin-polarized electrons accumulated in n-Ga_2Se_3 through NSs and the δ-shaped barrier (spin filter). The efficiency of spin injection from FM to SC through the tunneling barrier and the degree of spin accumulation in SC can be determined by comprehensive studies of the spin-polarized transport in hybrid structures by optical and electrical methods. A comparison of the data obtained in such studies with the results of the study of the impedance of hybrid structures in an extended frequency range ($f > 4 \times 10^6$ Hz) will make it possible to determine the physical nature of relaxation processes observed at $T = 300$ K in impedance spectra of these structures in the high-frequency region.

ACKNOWLEDGMENTS

This study was supported in part by the Science and Technology Center in Ukraine (STCU), grant no. 3098.

REFERENCES

1. A. Fert, Usp. Fiz. Nauk **178**, 1336 (2008) [Phys. Usp. **51**, 1336 (2008)].
2. I. Zutic, J. Fabian, and S. Das Sarma, Rev. Mod. Phys. **76**, 323 (2004).
3. A. M. Bratkovsky, Rep. Progr. Phys. **71**, 026502 (2008).
4. T. Dietl, J. Appl. Phys. **103**, 07D111 (2008).
5. R. I. Dzhigoev, B. P. Zakharchenya, K. V. Kavokin, and M. V. Lazarev, Fiz. Tverd. Tela **45**, 2153 (2003) [Phys. Solid State **45**, 2255 (2003)].
6. V. F. Motsnyi, J. De Boeck, J. Das, W. Van Roy, G. Borghs, E. Goovaerts, and V. I. Safarov, Appl. Phys. Lett. **81**, 265 (2002).
7. A. T. Hanbicki, B. T. Jonker, G. Itskos, G. Kioseoglu, and A. Petrou, Appl. Phys. Lett. **80**, 1240 (2002).
8. X. Lou, C. Adelmann, M. Furis, S. A. Crooker, C. J. Palmstrom, and P. A. Crowell, Phys. Rev. Lett. **96**, 176603 (2006).
9. E. I. Rashba, Appl. Phys. Lett. **80**, 2329 (2002).
10. A. Koma, Thin Solid Films **216**, 72 (1992).
11. W. Jaegermann, C. Pettenkofer, and B. A. Parkinson, Phys. Rev. B **42**, 7487 (1990).
12. V. L. Bakumenko, Z. D. Kovalyuk, L. N. Kurbatov, V. G. Tagaev, and V. F. Chishko, Fiz. Tekh. Poluprovodn. **14**, 1115 (1980) [Sov. Phys. Semicond. **14**, 661 (1980)].
13. S. Shigetomi, T. Ikari, and H. Nakashima, J. Appl. Phys. **76**, 310 (1994).
14. J. Martinez-Pastor, A. Segura, J. L. Valdes, and A. Chevy, J. Appl. Phys. **62**, 1477 (1987).
15. R. Mamy, X. Zaoni, J. Barrau, and A. Chevy, Rev. Phys. Appl. **25**, 947 (1990).
16. W. C. Huang, S. H. Su, Y. K. Hsu, C. C. Wang, and C. S. Chang, Superlat. Microstruct. **40**, 644 (2006).
17. Y. Cui, R. Dupere, A. Burger, D. Johnstone, K. C. Mandal, and S. A. Payne, J. Appl. Phys. **103**, 013710 (2008).
18. S. Duman, B. Gurbulak, S. Dogan, and A. Turut, Microelectron. Eng. **86**, 106 (2009).
19. N. Jedrecy, R. Pinchaux, and M. Eddrief, Phys. Rev. B **56**, 9583 (1997).
20. Z. R. Dai and F. S. Ohuchi, Appl. Phys. Lett. **73**, 966 (1998).

21. M. Eddrief, Y. Wang, V. H. Etgens, D. H. Mosca, J.-L. Maurice, J. M. Jeorge, A. Fert, and S. Bourgognou, Phys. Rev. B **63**, 094428 (2001).
22. A. R. de Moraes, D. H. Mosca, N. Mattoso, J. L. Guimaraes, J. J. Klein, W. H. Shreiner, P. E. N. de Sousa, A. J. A. de Oliveira, M. A. Z. de Vasconcellos, D. Demaille, M. Eddrief, and V. H. Etgens, J. Phys.: Condens. Matter **18**, 1165 (2006).
23. V. V. Slynko, A. G. Khandozhko, Z. D. Kovalyuk, V. E. Slynko, A. V. Zaslonkin, M. Arciszewska, and W. Dobrowolski, Phys. Rev. B **71**, 245301 (2005).
24. N. T. Pokladok, I. I. Grigorchak, B. A. Lukianets, and D. I. Popovich, Fiz. Tverd. Tela **49**, 681 (2007) [Phys. Solid State **49**, 715 (2007)].
25. I. I. Grigorchak, A. I. Pelekhovich, and N. V. Volynskaya, Fiz. Tekh. Poluprovodn. **42**, 385 (2008) [Semiconductors **42**, 375 (2008)].
26. S. I. Drapak, V. I. Gavrilyuk, Z. D. Kovalyuk, and O. S. Litvin, Fiz. Tekh. Poluprovodn. **42**, 423 (2008) [Semiconductors **42**, 414 (2008)].
27. G. J. Hughes, A. McKinley, R. H. Williams, and I. T. McGovern, J. Phys. C: Sol. St. Phys. **15**, L159 (1982).
28. S. I. Drapak, A. P. Bakhtinov, S. V. Gavrylyuk, Z. D. Kovalyuk, and O. S. Lytvyn, Superlat. Microstruct. **44**, 563 (2008).
29. A. P. Bakhtinov, V. N. Vodop'yanov, E. I. Slyn'ko, and Z. D. Kovalyuk, Pis'ma Zh. Tekh. Fiz. **33** (2), 80 (2007) [Tech. Phys. Lett. **33**, 86 (2007)].
30. H. S. Venugopalan, S. E. Mohney, B. P. Luther, S. D. W. Wolfer, and J. M. Redwing, J. Appl. Phys. **82**, 650 (1997).
31. P. Nielsen and J. J. Ritsko, J. Appl. Phys. **49**, 632 (1978).
32. A. I. Balitskii, A. S. Krochuk, I. M. Stakhira, and A. V. Franiv, Fiz. Tverd. Tela **24**, 76 (1982) [Sov. Phys. Solid State **24**, 42 (1982)].
33. V. Vasyltsiv, V. Kutsai, V. Savchyn, and Ya. Eiyala, Ukr. Phys. J. **44**, 1380 (1999).
34. V. M. Koshkin, *Current Problems in the Chemistry and Physics of Complex Semiconductor Compounds* (Uzhgorod, 1970), p. 26 [in Russian].
35. M. Peressi and A. Basdereschi, J. Appl. Phys. **83**, 3092 (1998).
36. V. Chican and D. F. Kelley, Nano Lett. **2**, 141 (2002).
37. D. A. Schmidt, T. Ohta, C. Y. Lu, A. A. Bostwick, O. Yu, E. Rotenberger, F. S. Ohuchi, and M. A. Olmstead, Appl. Phys. Lett. **88**, 181903 (2006).
38. A. Tsormapatzoglou, D. H. Tassis, C. A. Dimitriadis, L. Dozsca, N. G. Galkin, D. L. Goroshko, V. O. Polyarnyi, and E. A. Chusovitin, J. Appl. Phys. **100**, 074313 (2006).
39. R. T. Tung, Phys. Rev. B **45**, 13509 (1992).
40. S. I. Drapak, V. B. Orletskii, Z. D. Kovalyuk, and V. V. Netyaga, Fiz. Tekh. Poluprovodn. **37**, 196 (2003) [Semiconductors **37**, 187 (2003)].
41. M. Di Giulio, G. Micocci, and A. Tepore, Solid State Electron. **27**, 1015 (1984).
42. P. N. Brunov, A. A. Suvorova, N. A. Berg, A. F. Kovsh, A. E. Zhukov, A. Yu. Egorov, V. M. Ustinov, A. F. Tsatsul'nikov, N. N. Ledentsov, P. S. Kop'ev, S. G. Konnikov, L. Ivs, and P. S. Mains, Fiz. Tekh. Poluprovodn. **32**, 1229 (1998) [Semiconductors **32**, 1096 (1998)].
43. S. D. Lin, V. V. Ilchenko, V. V. Marin, N. N. Shkil, A. A. Buyanin, K. Y. Panarin, and O. V. Tretyak, Appl. Phys. Lett. **90**, 263114 (2006).
44. A. K. Jonscher, C. Pickup, and S. H. Zaidi, Semicond. Sci. Technol. **1**, 71 (1986).
45. M. Matsumura and Y. Hirose, Appl. Surf. Sci. **175–176**, 740 (2001).
46. J. D. Albrecht and D. L. Smith, Phys. Rev. B **68**, 035340 (2003).
47. V. V. Osipov and A. M. Bratkovsky, Appl. Phys. Lett. **84**, 2118 (2004).
48. A. M. Bratkovsky and V. V. Osipov, J. Appl. Phys. **96**, 4525 (2004).
49. Yu. V. Pershin, Phys. Rev. B **77**, 073301 (2008).
50. A. G. Petukhov, J. Niggemann, V. N. Smelyanskiy, and V. V. Osipov, J. Phys.: Condens. Matter **19**, 315205 (2007).
51. M. Ershov, H. C. Liu, L. Li, M. Buchanan, Z. R. Wasilewski, and A. K. Jonscher, IEEE Trans. Electron. Dev. **45**, 2196 (1998).
52. J. Werner, A. F. J. Levi, R. T. Tung, M. Anzlovar, and M. Pinto, Phys. Rev. Lett. **60**, 53 (1988).
53. W. Huang, J. Peng, L. Wang, J. Wang, and Y. Cao, Appl. Phys. Lett. **92**, 013308 (2008).
54. A. J. Chiquito, Yu. A. Pusep, S. Mergulhao, J. S. Galzerani, N. T. Moshegov, and D. L. Miller, J. Appl. Phys. **88**, 1987 (2000).
55. Y. Y. Proskuryakov, K. Durose, B. M. Taele, and S. Oelting, J. Appl. Phys. **102**, 025504 (2007).
56. W. Rudzinski and J. Barnas, Phys. Rev. B **64**, 085318 (2001).
57. P. W. Li, W. M. Liao, D. M. T. Kuo, S. W. Lin, P. S. Chen, S. C. Lu, and M. J. Tsai, Appl. Phys. Lett. **85**, 1532 (2004).
58. I. Weymann and J. Barnas, Phys. Rev. B **77**, 075305 (2008).
59. J. C. A. Huang and H. S. Hsu, Appl. Phys. Lett. **87**, 132503 (2005).

Translated by A. Kazantsev